Enhancement of plasma illumination characteristics of few-layer graphenediamond nanorods hybrid

Peer-reviewed author version

KAMATCHI JOTHIRAMALINGAM, Sankaran; Yeh, Chien-Jui; DRIJKONINGEN, Sien; POBEDINSKAS, Paulius; VAN BAEL, Marlies; Leou, Keh-Chyang; Lin, I-Nan & HAENEN, Ken (2017) Enhancement of plasma illumination characteristics of few-layer graphenediamond nanorods hybrid. In: NANOTECHNOLOGY, 28(6) (Art N° 065701).

DOI: 10.1088/1361-6528/aa5378
Handle: http://hdl.handle.net/1942/23002

Enhancement of plasma illumination characteristics of few-layer graphene–diamond nanorods hybrid

Kamatchi Jothiramalingam Sankaran[1,2], Chien-Jui Yeh[3], Sien Drijkoningen[1,2], Paulius Pobedinskas[1,2], Marlies K. Van Bael[1,2], Keh-Chyang Leou[3], I-Nan Lin[4] and Ken Haenen[1,2]

[1] Institute for Materials Research (IMO), Hasselt University, Diepenbeek, Belgium.

[2] IMOMEC, IMEC vzw, Diepenbeek, Belgium.

[3] Department of Engineering and System Science, National Tsing Hua University, Hsinchu, Taiwan, Republic of China.

[4] Department of Physics, Tamkang University, Tamsui, Taiwan, Republic of China.

Email: sankaran.kamatchi@uhasselt.be and ken.haenen@uhasselt.be

Keywords: few-layer graphene, diamond nanorods, field electron emission, plasma illumination

Supplementary material for this article is available online

Abstract

Few-layer graphene (FLG) was catalytically formed on vertically aligned diamond nanorods (DNRs) by a high temperature annealing process. The presence of 4–5 layers of FLG on DNRs was confirmed by transmission electron microscopic studies. It enhances the field electron emission (FEE) behavior of the DNRs. The FLG-DNRs show excellent FEE characteristics with a low turn-on field of 4.21 V/μm and a large field enhancement factor of 3480. Moreover, using FLG-DNRs as cathode markedly enhances the plasma illumination behavior of a microplasma device, viz. not only the plasma current density is increased, but also the robustness of the devices is improved.

---

1. Introduction

Graphene, a two dimensional carbon honeycomb lattice, has attracted remarkable attention from both experimental and theoretical communities since its first exfoliation from graphite in 2004 [1]. The highly desirable properties of graphene, such as atomic thickness, excellent electrical and thermal conductivity, good mobility of charge carriers, superior chemical stability, high aspect ratio and sharp edges, make it a prospect material for field electron emission (FEE) applications [2–7]. Graphene hybrid nanostructures have been explored extensively since the past decade for their effectual FEE performances [8–12]. Highly efficient field emitters based on monolayer graphene coated on Si tip arrays fabricated by a simple transfer method, have been demonstrated [13]. Enhanced FEE behavior is also observed by depositing graphene on the surface of zinc oxide nanowires and carbon nanotubes [14, 15]. However, the FEE efficiency from flat sheets of graphene synthesized using electrophoretic deposition and chemical vapor deposition (CVD) methods is insufficient, because electrons emit only from the sharp edges of graphene [16–18]. In addition, the short lifetime and poor stability of the graphene emitters in a plasma environment averted them to be used in practical applications.

Diamond with a strong covalently bonded crystal structure and a high negative electron affinity, when hydrogen terminated [19, 20], is a candidate field electron source with high lifetime and reliability. Furthermore, diamond promises a large secondary electron emission efficiency, which would make it particularly suitable as a cathode material in plasma-based devices [21]. Therefore, it is well-intentioned to combine graphene and diamond nanostructures to form hybrids for better FEE characteristics, as such hybrids are envisaged to have the advantages of both high stability of diamond and the sharp edges of the graphene layers.

However, there has only been limited success regarding the growth of graphene layers on diamond [22–24]. The probable cause which results in non-satisfactory FEE behavior for these hybrid materials is that the coating of graphene on diamond usually induces a large discontinuity in carbon bonding at the diamond-to-graphene interface that hampers the transport of electrons crossing the said interface. According to theoretical calculations, rearrangement of the carbon atoms at the outermost layer of diamond nanostructures is expected to cause a structural transformation from diamond to graphene nanoribbons [25, 26]. Recent reports succeed in the formation of graphene layers experimentally on diamond via a high temperature annealing method [27–29].

In this paper, we demonstrated the fabrication of hybrid field emitters using a simple and efficient method for the formation of few-layer graphene (FLG) on diamond nanorods (DNRs). Practically, these hybrid field emitters can be used as electron sources for advanced devices. We observed noticeable improvements in the FEE behavior for the FLG-DNRs emitting materials and marked enhancement of the plasma illumination (PI) characteristics of the fabricated microplasma devices, which used the FLG-DNRs hybrids as the cathodes.

2. Experimental section

The schematic description of the fabrication process for FLG-DNRs is illustrated in figure 1. Nanocrystalline diamond (NCD) films were first grown on *n*-type Si substrates using an ASTeX 6500 series microwave plasma enhanced chemical vapor deposition system (figure 1(a)). Prior to NCD deposition, the Si substrates were cleaned with sulfuric acid/hydrogen peroxide and ammonia/hydrogen peroxide mixtures. The substrates were then seeded using a colloidal suspension containing nanodiamond (ND) particles (~5 nm in diameter) and deionized water.

The NCD films were deposited using a CH_4 (6%)/H_2 (91%)/N_2 (3%) plasma with a microwave power of 3000 W for 5 h. The pressure and the flow rate were maintained at 30 Torr and 300 sccm, respectively. The substrates were heated up due to the bombardment of the plasma species and the growth temperature to around 540°C during the growth of NCD films. The growth temperature was measured using an optical pyrometer.

The NCD films were then immersed in the ND colloidal suspension and sonicated for 10 min to deposit ND particles, which act as a mask on the films surface (figure 1(b)). Subsequently, the masked NCD film was subjected to a reactive ion etching (RIE) process in an O_2 plasma at a DC pulsed power of 200 W for 30 min to fabricate DNRs (figure 1(c)). A 150 nm thick copper layer was coated on the obtained DNRs by DC-pulsed sputtering using a power of 450 W in Ar pressure of 4 mTorr (figure 1(d)). The copper coated DNRs were subjected to thermal annealing at 800°C for 1 h under vacuum (3×10^{-5} Torr; typical base pressure: 2×10^{-6} Torr), followed by cooling down to room temperature at a controlled rate of 0.5°C/min. The copper coating was then etched away using nitric acid, resulting in FLG-DNRs hybrids (figure 1(e)).

The morphology and the microstructure of FLG-DNRs hybrids were characterized by scanning electron microscopy (SEM; FEI Quanta 200 FEG microscope) and transmission electron microscopy (TEM; JEOL 2100F), respectively. Raman spectra were performed on a confocal micro-Raman spectroscopy (Horiba Jobin-Yvon T64000 spectrometer; with a 488.0 nm laser with spot size ~1 μm; laser power=400 mW, time=180 s per measurement, 10 times measured for averaging, 150 points for overlapping the measured spectra windows). FEE characteristics of the samples were measured using a parallel-plate setup, which used a Mo rod with a diameter of 2 mm as anode and FLG-DNRs (DNRs) as cathode. The cathode-to-anode

distance was controlled by a micrometer and the distances were 98 μm when measuring the FEE properties of FLG-DNRs and 66 μm for DNRs. The *I-V* characteristics were acquired using a Keithley 2410 electrometer (Keithley Instruments, Inc., OH, USA). The FEE behavior of the materials was modeled using Fowler-Nordheim (F-N) theory [30], $J_e = \left(\frac{A\beta^2E^2}{\varphi}\right)\exp\left(-\frac{B\varphi^{\frac{3}{2}}}{\beta E}\right)$, where $A = 1.54 \times 10^{-6}$ A eV/V^2 and $B = 6.83 \times 10^9$ eV$^{-3/2}$ V/m, β is the field-enhancement factor, E is the applied field, J_e is the FEE current density and φ is the work function of the emitting materials. The intersection of the straight lines extrapolated from the high-field and low-field segments of the F-N plot was designated as turn-on field (E_0). Moreover, the suitability of these FLG-DNRs for the application as cathode materials for a microplasma device was investigated. The fabrication of microplasma device using FLG-DNRs as cathode is given elsewhere [31]. Briefly, the microplasma device was fabricated using indium tin oxide coated glass as the anode and FLG-DNRs as the cathode. The cathode-to-anode separation was fixed by a polytetrafluoroethylene spacer (1.0 mm in thickness), which includes a circular hole of about 3.0 mm in diameter as plasma cavity. The plasma was triggered using a pulse dc mode (a 20 ms square pulse and a 6 kHz repetition rate) in Ar environment (2 Torr).

3. Results

A SEM image of the NCD films (inset of figure 2(a)) shows a dense and uniform nano-grain microstructure with very smooth surface. The thickness of the films is about 600 nm. Figure 2(a) shows the tilted SEM image of the vertically aligned DNRs with diameters of ~50 nm and lengths of ~250 nm. The thickness of the pristine NCD film and the length of the DNRs were estimated using cross-sectional SEM images (figures not shown). Figure 2(b) shows that the morphology of FLG-DNRs is similar to the DNRs before FLG growth. The SEM image taken

from the top of the FLG-DNRs (inset of figure 2(b)) reveals that the nanorods are evenly distributed and the separation between each DNR is ~150 nm.

The bonding structure of the samples was examined using confocal micro-Raman spectroscopy. Both of the Raman spectra of the pristine DNRs (spectrum I, figure 2(c)) and FLG-DNRs (spectrum II, figure 2(c)) contain D-band (~1360 cm^{-1}) and G-band (~1561 cm^{-1}) resonance peaks, which correspond to disordered carbon and graphite [32–35], respectively, and the v_1-band (~1140 cm^{-1}) and v_3-band (~1489 cm^{-1}) resonance peaks, which corresponds to the deformation modes of CH_x bonds in the DNRs [36]. The diamond resonance peak at 1332 cm^{-1} (labeled as "dia", figure 2(c)) corresponds to the F_{2g} resonance mode of the 3C diamond lattice. Notably, a broad 2D band around 2700 cm^{-1} (spectrum II, figure 2(d)) originates from a second order process, signifying the formation of graphene-like materials for FLG-DNRs [17]. No signal for graphene is observed in the second order Raman spectrum of the DNRs (spectrum I of figure 2(d)). The full width at half maximum of the 2D band is about ~64 cm^{-1}, implying that the thickness of the coating on the DNRs corresponds to a few layers of graphene [4, 37, 38]. It should be mentioned that the D, G and 2D bands in figures 2(c) and 2(d) are not as narrow as conventional "few layer graphene". This can be ascribed to the presence of large proportion of defects in these graphene-like materials. To facilitate the comparison, DNRs were annealed at 800°C without copper coating and the corresponding Raman spectrum is shown in supporting information (figure S1). There is no evidence of the 2D band in the second order Raman spectrum (inset, figure S1), revealing the absence of graphene layers when the bare DNRs were annealed. This confirms that the Cu-coating is necessary for forming graphene-like materials on DNRs via annealing process.

TEM was performed to study the microstructure of FLG-DNR materials. The high resolution TEM (HRTEM) image of a single DNR (figure 2(e)), which was taken from the region marked as "I" in the bright field (BF) TEM micrograph for FLG-DNRs (inset of figure 2(e)) reveals the presence of two crystalline carbon phases in these materials, i.e., diamond with a lattice spacing of 0.21 nm (region "A", figure 2(e)) and graphene-like materials with a lattice spacing of 0.33 nm (region "B", figure 2(e)). The formation of graphene–like materials with a thickness of ~2 nm, corresponding to 4–5 layers, over the whole FLG-DNR surface is confirmed (figure 2(e)). Furthermore, the Fourier transformed diffractogram corresponding to the region "A" of the structure image (FT_A) clearly illustrated the presence of (111) diffraction spots, confirming the nature of diamond phase for the materials in region "A", whereas the FT image corresponding to the region "B" (FT_B) indicates that these curved parallel fringes correspond to (0002) diffraction spots of graphite materials, assuring the graphene-like nature of the materials for region "B". Notably, the (0002) lattice planes of graphene-like materials were in parallel with the (111) lattice plans of diamond materials. There is no interfacial phase located in between them. The continuous transition of the lattice planes is expected to facilitate the transport of electrons among these two phases. The HRTEM image in figure 2(f) taken from the region marked "II" in the BF TEM micrograph (inset of figure 2(e)) shows the presence of a few parallel layers of graphene-like materials, covering the DNRs. Moreover, a detailed investigation on the microstructure of the FLG-DNRs from other regions of FLG-DNRs materials were illustrated as another sets of TEM micrographs, which were shown in supporting information (figures S2 and S3), confirming that graphene-like materials conformally cover the whole DNRs.

The FEE measurements for the FLG-DNRs and the pristine DNRs are shown in figure 3(a). The $ln(J_e/E^2)$ versus $1/E$ plot is illustrated in figure 3(b) to indicate that the FEE behavior of

these materials can be modeled by F-N equation. The FLG-DNRs require only a small field of $(E_0)_{FLG\text{-}DNRs}$ = 4.21 V/μm to turn on the FEE process and reach a FEE current density of $(J_e)_{FLG\text{-}DNRs}$ = 2.24 mA/cm^2 at an applied field of E=10.0 V/μm (curve II of figure 3(a)). Such FEE properties are markedly superior to those of the pristine DNRs with $(E_0)_{DNRs}$=7.26 V/μm and $(J_e)_{DNRs}$=0.60 mA/cm^2 at E=15.1 V/μm (curve I of figure 3(a)). The corresponding β values can be estimated from the slope (m) of F-N plots, using $\beta = [-6.8 \times 10^3 \varphi^{3/2}]/m$. The β values corresponding to the FLG-DNRs and the pristine DNRs were estimated to be $(\beta)_{FLG\text{-}DNRs}$ = 3480 and $(\beta)_{DNRs}$ = 2326, respectively, by taking the φ values as 3.5 eV for FLG-DNRs [39, 40], and 5.0 eV for DNRs [41]. Notably, the φ=3.5 eV instead of 5.0 eV was assumed for FLG-DNRs, since the FLG-DNRs contain few layer graphene phases encasing the DNRs [39, 40]. The FLG-DNRs exhibit far more superior FEE properties than that of pristine DNRs. The FEE characteristics of FLG-DNRs are comparable with those of the other graphene coated field emitting nanostructures reported in literature [13–15, 42–44], which are summarized in table 1.

Superior FEE materials by themselves possess great potential for applications, such as electron sources for FEE-based flat panel display, travelling wave tube amplifier or portable X-ray tube, etc. [2–7]. However, other applications such as microplasma devices might be as useful and versatile as any other kind of devices. Microplasma based devices signify a photonics based technology at the interfaces of plasma science, optoelectronics, and materials science. The plasma-based devices show a promising future applied to a broad spectrum related to microdisplays, detectors of environmentally hazardous gases or vapors, and tools for elemental analysis. In the operation of a microplasma device, the stability of the plasma is of paramount importance. Thus, materials with a large secondary electron emission efficiency and good

robustness (long lifetime and reliability) are urgently needed for serving as cathode for these devices [21]. Moreover, simulations by Venkataraman *et al.* [45, 46] predicted that cathode materials with efficient electron emission capability can improve microplasma device characteristics markedly. Therefore, FLG-DNRs materials with good FEE properties were thus tested for the possibility of being a good cathode for a microplasma device. That is, the plasma illumination (PI) characteristics of a microplasma device employing FLG-DNRs (or DNRs) as cathode were investigated.

The schematic of the configuration for microplasma devices under test is shown as inset in figure 4(a), where the plasma current versus applied voltage (V) was measured using the Keithley 237 electrometer. Figure 4(a) shows the variation of plasma current density against the applied voltage, the J_{PI}-V curves, indicating that the J_{PI}-value increases monotonically with the applied voltage for both FLG-DNRs- and pristine DNRs-based microplasma devices. Curve I in figure 4(a) illustrates that the pristine DNRs-based microplasma device requires 600 V to trigger the plasma and a $(J_{PI})_{DNRs}$ value of 12.5 mA/cm^2 was attained at an applied voltage of 900 V. In contrast, curve II in figure 4(a) indicates that the FLG-DNRs-based microplasma device can be triggered at a lower voltage of 540 V and a higher $(J_{PI})_{FLG\text{-}DNRs}$ of 14.8 mA/cm^2 was achieved at the same applied voltage. A sequence of photographs of the PI image of the microplasma devices, which utilized the pristine DNRs and FLG-DNRs as cathodes, were shown in image series I and II of figure 4(b), respectively.

The fascinating phenomenon is that the FLG-DNRs based microplasma device not only shows better PI behavior than the pristine DNRs cathode-based device, it also exhibits superior robustness. To evaluate the stability of a cathode material, the J_{PI}-value of the corresponding microplasma devices was monitored with a constant applied voltage of 650 V (figure 4(c)). The

J_{PI}-value of the pristine DNRs-based microplasma device decays after 938 s (curve I, figure 4(c)), at which point the intensity of the PI drops abruptly. The bottom inset of figure 4(c) illustrates the corresponding PI images. Interestingly, for the FLG-DNRs-based microplasma device, the plasma current can be upheld for longer period of 1210 s (curve II, figure 4(c)) and the PI intensity (at 650 V) remains essentially the same (upper inset, figure 4(c)). It should be noted that FLG-DNRs-based microplasma devices was tested under larger plasma current density than the DNRs-based ones, when tested under the same applied voltage (650 V), i.e., the pristine DNRs-based microplasma device shows 3.5 mA/cm^2 and the FLG-DNRs-based microplasma device exhibits 5.3 mA/cm^2. The total output power density for the microplasma before failure, which is $W=J_{PI} \cdot V \cdot t$, is 1.97 kW/cm^2 for DNRs-based and is 3.85 kW/cm^2 for FLG-DNRs-based microplasma devices. The output power density of FLG-DNRs based device is twice as much as that for the DNRs-based device. These results signify that the FLG-DNRs hybrid provides a better cathode material compared with the pristine DNRs.

It is to be noted that the cathode material in the microplasma device experienced continuous bombardment of Ar-ions with high kinetic energies (>400 eV) that is conceived as the harshest environment in the device applications. The above described results indicate that the formation of FLG on DNRs not only enhances the FEE properties of the DNRs, but also improves the robustness of these materials against the plasma ion bombardments when they were used as cathode materials in a microplasma device. This is a rather unusual combination of characteristics. Usually, the stand alone graphene materials, which are made of hexagons with sp^2-bonded carbons, are not resistant to bombardment damage of plasma ions, compared to diamond.

4. Discussion

An interesting but a puzzling phenomenon is the influence of the cathode materials on the behavior of a microplasma device. The microplasma device is typically operated at around 650 V, which corresponds to an electrical field of 0.65 V/μm for an anode-to-cathode spacing of 1 mm. Such an applied field is almost one order of magnitude less than the turn-on field required for initiating the FEE process for either FLG-DNRs materials with $(E_0)_{\text{FLG-DNRS}}$ = 4.21 V/μm or DNRs materials with $(E_0)_{\text{DNRS}}$ = 7.26 V/μm. Why the microplasma devices using FLG-DNRs as cathode show superior plasma current density to the ones using DNRs as cathode (cf. Fig. 4(b))? To understand the possible mechanism behind such a phenomenon, the plasma process of a device need to be addressed. Usually, plasma contains abundant electrons and ions in addition to the neutral species (such as Ar). The plasma loses the electrons and ions continuously due to bombardment of these charged particles with electrodes (anodes and cathodes) and walls of container. Therefore, it needs continuous replenish of electron-ion pairs. Conventionally, this is done by the supplement of secondary electrons emitted from the cathode, as these electrons can be accelerated by the bias voltage and subsequently ionize the plasma species (Ar) to produce new electron-ion pairs. The materials with high efficiency for producing secondary electrons, i.e., large secondary electron emission co-efficient materials, such as diamond, are thus favored for the choice of cathode materials. Even when a plasma sheath of the thickness around tens of microns were formed near the cathode in a plasma that increased abruptly the electric field experienced by cathode, such a field might still not large enough to initiate the FEE process for the FLG-DNRs (or DNRs). The more probable factor is the slight increase in coefficient of

secondary electron emission (γ-coefficient) due to the formation of FLG on DNRs. The reason for the increase in γ-coefficient for DNRs due to FLG coating is still not fully understood yet.

The other issue, which needs clarification, is why the formation of FLG, which is intrinsically susceptible to plasma ion bombardment damage, on DNRs can enhance the lifetime for the cathode material during the microplasma operation. The possible explanation for such a phenomenon is that in a microplasma device, the plasma sheath formed only in the regions nearby the electron emission sites, which are located at the tip of DNRs. Hence, only the graphene-like materials in these regions of FLG-DNRs were eroded by the plasma ions, whereas the graphene-like materials coated on the side walls of FLG-DNRs remained intact. The side wall of DNRs can still transport electrons efficiently upward, transferring them to the tip of DNRs and then field emitted.

On the other hand, the explanation on how the formation of FLG on DNRs enhanced the FEE properties of these materials is not as straightforward. First of all, the fabrication of nanorods is expected to increase significantly the field enhancement factor (β-value) of the NCD films due to the high aspect ratio of the nanostructures, resulting in markedly better FEE properties for DNRs compared with those of NCD films. Moreover, the transport of electrons from the bottom of the DNRs vertically toward their tips will be greatly improved due to conformal coating of FLG on DNRs, as FLG with hexagonal carbon lattices is extremely conductive. The other possible mechanism is the nanoscale dielectric inhomogeneity proposed by Carey's and Ilie's groups [47–49]. They demonstrated that sp^2 clusters embedded in the sp^3 matrix or electronic disorder induced by localized defects oriented in the field direction can provide a local field enhancement to facilitate the emission. As a consequence, in the present

FLG-DNRs, conductive sp^2-graphene phase surrounding the sp^3-DNRs, giving rise to dielectric inhomogeneity that lead to an enhanced local field at the tip as implied by the high β-value for FLG-DNRs.

However, the electrons still need to transfer from the graphene to diamond at the tip of FLG-DNRs for field emission. It should be noted that in the case where graphene layers were coated on other kind of sharp templates such as Si-tip arrays [13], Si nano-rod arrays [15] and TiO_2/diamond like carbon (DLC) films [41], the electrons conducted by the graphene layers could not be efficiently transferred to the emission sites due to the presence of larger barrier between the graphene and the underlying substrate materials. The graphene layers thus did not contribute much to FEE process for these materials, Here it is proposed that the formation of FLG on DNRs *in-situ* can enhance the overall FEE behavior of the materials because the electrons x can be transferred from the FLG to the DNRs easily, since the FLG was formed via *in-situ* annealing process. There exists intimated connection of (0002) lattice planes of FLG with (111) lattice planes of diamond materials. This is not happening when the graphene-like materials were separately formed by CVD growth and then coated on templates by post-growth transferring processes. In the *in-situ* formation of FLG on DNRs, the carbon species were assumed to diffuse from the DNRs to the Cu coating, dissolved in Cu, during the annealing step and then re-precipitated out during the cooling down step, a process similar to the CVD synthesis of graphene using Cu substrates [27]. The outward diffused carbons (from Cu coating) are very active and can form carbon hexagons on surface of DNRs that created a clean interface between these two forms of carbon, graphene-like materials and diamond. This proposed formation mechanism is supported by the TEM observation (cf. figure 2(e)) that the (111) lattice planes of diamond transit to the (0002) lattice planes of graphene without the formation of an amorphous

carbon interface layer. Therefore, aside from the difference in Fermi level in the FLG and the DNRs, the electrons can transfer between the two materials without a large barrier.

5. Conclusion

In summary, an effective approach to fabricate a hybrid structure of FLG coated DNRs for enhanced FEE and microplasma illumination device applications has been successfully demonstrated. The FLG conformally covers the DNRs with 4–5 layer sharp edges. The FLG-DNRs hybrid displays excellent FEE properties, with $(E_0)_{\text{FLG-DNRs}}$ =4.21 V/μm, $(J_e)_{\text{FLG-DNRs}}$ = 2.24 mA/cm^2 at an applied field of E=10 V/μm and $(\beta)_{\text{FLG-DNRs}}$ = 3480, which are much better than those of the pristine DNRs: ($(E_0)_{\text{DNRs}}$=7.26 V/μm, $(J_e)_{\text{DNRs}}$=0.60 mA/cm^2 at E=15.1 V/μm and $(\beta)_{\text{DNRs}}$ =2326). The PI characteristics of the microplasma devices were markedly enhanced by using these hybrids as cathode materials, which is closely related to their superior FEE characteristics. The FLG-DNRs hybrid-based microplasma devices show a J_{PI} value of 14.8 mA/cm^2 at V= 900 V and a prolonged plasma lifetime stability of 1210 s at an operating current density of 5.3 mA/cm^2 with a stable plasma intensity, as compared to that of the pristine DNRs (J_{PI}=12.5 mA/cm^2 at V= 900 V and plasma lifetime stability of 938 s) at 5.3 mA/cm^2 operating current density. This distinctive structure confirms full usage of the advantages of DNRs and FLG during FEE and PI processes. Therefore, it can be concluded that FLG-DNRs hybrids are more promising materials for field emission and microplasma display applications.

Acknowledgements

The authors like to thank the financial support of the Research Foundation Flanders (FWO) via Research Projects G.0456.12N and G.0905.12N, and the Methusalem “NANO” network.

Kamatchi Jothiramalingam Sankaran and Paulius Pobedinskas are Postdoctoral Fellows of the Research Foundation-Flanders (FWO).

References

[1] Novoselov, K S, Geim, A K, Morozov, S V, Jiang, D, Zhang Y, Dubonos S V, Grigorieva I V and Firsov A A 2004 Electric field effect in atomically thin carbon films *Science* **306** 666–69.

[2] Geim A K and Novoselov K S 2007 The rise of graphene *Nat. Mater.* **6** 183–91.

[3] Kopelevich Y and Esquinazi P 2007 Graphene physics in graphite *Adv. Mater.* **19** 4559–63.

[4] Qian M, Feng T, Ding H, Lin L, Li H, Chen Y and Sun Z 2009 Electron field emission from screen printed graphene films *Nanotechnology* **20** 425702.

[5] Malesevic A, Kemps R, Vanhulsel A, Chowdhury M P, Volodin A and Haesendonck C V 2008 Field emission from vertically aligned few-layer graphene *J. Appl. Phys.* **104** 084301.

[6] Zhang Y, Tang S, Deng D L, Deng S Z, Chen J and Xu N S 2013 Growth direction manipulation of few-layer graphene in the vertical plane with parallel arrangement *Carbon* **56** 103–8.

[6] Todorovic D, Matkovic A, Milicevic M, Jovanovic D, Gajic R, Salom I and Spasenovic M 2015 Multilayer graphene condenser microphone *2D Mater.* **2** 045013.

[7] Huang C K, Ou Y X, Bie Y Q, Zhao Q and Yu D P 2011 Well-aligned graphene arrays for field emission displays *Appl. Phys. Lett.* **98** 263104.

[8] Ye D, Moussa S, Ferguson J D, Baski A A and Samy El-Shall M 2012 Highly efficient electron field emission from graphene oxide sheets supported by nickel nanotip arrays *Nano Lett.* **12** 1265–68.

[9] Devarapalli R R, Kashid R V, Deshmukh, A B, Sharma P, Das M R, More M A and Shelke M V 2013 High efficiency electron field emission from protruded graphene oxide nanosheets supported on sharp silicon nanowires *J. Mater Chem. C* **1** 5040–46.

[10] Zou R, He G, Xu K, Liu Q, Zhang Z and Hu J 2013 ZnO nanorods on reduced graphene sheets with excellent field emission, gas sensor and photocatalytic properties *J. Mater Chem. A* **1** 8445–52.

[11] Lei W, Li C, Cole M T, Qu K, Ding S, Zhang Y, Warner J H, Zhang X, Wang B and Milne W I 2013 A graphene-based large area surface-conduction electron emission display *Carbon* **56** 255–63.

[12] Samori P, Kinloch I A, Feng X, and Palermo V 2015 Graphene-based nanocomposites for structural and functional applications: using 2-dimensional materials in 3-dimensional world *2D Mater.* **2** 030205.

[13] Chang T, Lu F, Kunuku S, Leou K, Tai N and Lin I 2015 Enhanced electron field emission properties from hybrid nanostructures of graphene/Si tip array *RSC Adv.* **5** 2928–33.

[14] Zheng W T, Ho Y, Tian H, Wen M, Qi J and Li Y 2009 Field emission from a composite of graphene sheets and ZnO nanowire *J. Phys Chem. C* **113** 9164–68.

[15] Deng J H, Zheng R T, Yang Y M, Zhao Y and Cheng G 2012 Excellent field emission characteristics from few-layer graphene-carbon nanotube hybrids synthesized using radio frequency hydrogen plasma sputtering deposition *Carbon* **50** 4732–37.

[16] Wei Z, Pei S, Ren W, Tang D, Gao L, Liu B, Li F, Liu C and Cheng H M 2009 Field emission of single-layer graphene films prepared by electrophoretic deposition *Adv. Mater.* **21** 1756–60.

[17] Li X, Cai W, An J, Kim S, Nah J, Yang D, Piner R, Velamakanni A, Jung I, Tutuc E, Banerjee S K, Colombo L and Ruoff R S 2009 Large-area synthesis of high-quality and uniform graphene films on copper foils *Scienc*e **324** 1312–14.

[18] Yamaguchi H, Murakami K, Eda G, Fujita T, Guan P and Wang W 2011 Field emission from atomically thin edges of reduced graphene oxide *ACS Nano* **5** 4945–52.

[19] Yamaguchi H, Masuzawa T, Nozue S, Kudo Y, Saito I, Koe J, Kudo M, Yamada T, Takakuwa T and Okano K 2009 Electron emission from conduction band of diamond with negative electron affinity *Phys. Rev. B* **80** 165321.

[20] Geis M W, Deneault S, Krohn K E, Marchant M, Lyszczarz T M and Cooke D L 2005 Field emission at 10V cm^{-1} with surface emission cathodes on negative-electron affinity insulators *Appl. Phys. Lett.* **87** 192115.

[21] Kunuku S, Sankaran K J, Dong C L, Tai N H, Leou K C and Lin I N 2014 Development of long lifetime cathode materials for microplasma application *RSC Adv.* **4** 47865–75.

[22] Garcia J M, He R, Jiang M P, Kim P, Pfeiffer L N and Pinczuk A 2011 Multilayer graphene grown by precipitation upon cooling of nickel on diamond *Carbon* **49** 1006.

[23] Tzeng Y, Chen W L, Wu C, Lo J Y and Li C Y 2013 The synthesis of graphene nanowalls on a diamond film on a silicon substrate by direct-current plasma chemical vapor deposition *Carbon* **53** 120–9.

[24] Varshney D, Rao C, Guinel M, Ishikawa Y, Weiner B and Morell G 2011 Freestanding graphene-diamond hybrid films and their electron emission properties *J. Appl. Phys.* **110** 044324.

[25] Okada S 2009 Formation of graphene nanostructures on diamond nanowire surfaces *Chem. Phys. Lett.* **483** 128–32.

[26] Hu W, Li Z and Yang J 2013 Diamond as an inert substrate of graphene *J. Chem Phys.* **138** 054701.

[27] Ueda K, Aichi S and Asano H 2016 Direct formation of graphene layers on diamond by high-temperature annealing with a Cu catalyst *Diamond and Relat. Mater.* **63** 148–52.

[28] Tokuda N, Fukui M, Makino T, Takeuchi D, Yamsaki S and Inokuma T 2013 Formation of graphene-on-diamond structure by graphitization of atomically flat diamond (111) surface *Jap. J. Appl. Phys.* **52** 110121.

[29] Ogawa S, Yamada T, Ishizduka S, Yoshigoe A, Hasegawa M, Teraoka Y and Takakuwa Y 2012 Vacuum annealing formation of graphene on diamond C(111) surfaces studies by real-time photoelectron spectroscopy *Jap. J. Appl. Phys.* **51** 11PF02.

[30] Fowler R H and Nordheim L 1928 Electron emission in intense electric fields *Proc. R. Soc. London, Ser. A.* **119** 173–81.

[31] Sankaran K J, Kunuku S, Lou S C, Kurian J, Chen H C, Lee C Y, Tai N H, Leou K C, Chen C and Lin I N 2012 Microplasma illumination enhancement of vertically aligned conducting ultrananocrystalline diamond nanorods *Nanoscale Research Lett.* **7** 522.

[32] Ferrari A C and Robertson J 2001 Origin of the 1150 cm^{-1} Raman mode in nanocrystalline diamond *Phys. Rev. B* **63** 121405.

[33] Michler J, von Kaenel Y, Stiegler J and Blank E 1998 Complementary application of electron microscopy and micro-Raman spectroscopy for microstructure, stress, and bonding defect investigation of heteroepitaxial chemical vapor deposited diamond films *J. Appl. Phys.* **83** 187–97.

[34] Ferrari A C and Robertson J 2000 Interpretation of Raman spectra of disordered and amorphous carbons *Phys. Rev. B* **61** 14095.

[35] Ilie A, Ferrari A C, Yagi T, Rodil S E, Robertson J, Barborini E and Milani P 2001 Role of sp^2 phase in field emission from nanostructured carbons *J. Appl. Phys.* **90** 2024–32.

[36] Mortet V, Zhang L, Eckert M, Haen J D, Soltani A, Moreau M, Troadec D, Neyts E, Jaeger J C D, Verbeeck J, Bogaerts A, Tendeloo G V, Haenen K and Wagner P 2012 Grain size tuning of nanocrystalline chemical vapor deposited diamond by continous electrical bias growth: Experimental and theoretical study *Phys. Status Solidi A* **209** 1675–82.

[37] Lahiri I, Verma V P, Choi W 2011 An all-graphene based transparent and flexible field emission device *Carbon* **49** 1614–19.

[38] Zhu Y, Murali S, Cai W, Li X, Suk J W, Potts J R and Ruoff R S 2010 Graphene and graphene oxide:Synthesis, Properties, and Applications *Adv. Mater.* **22** 3906–24.

[39] Cui J B, Ristein J and Ley L 1999 Low-threshold electron emission from diamond *Phys. Rev. B* **60** 16135.

[40] Wang S G, Zhang Q, Yoon S F, Ahn J, Yang D J, Wang Q, Zhou Q and Li J Q 2003 Electron field emission from carbon nanotubes and undoped nano-diamond *Diamond Relat. Mater.* **12** 8–14.

[41] Liu J, Zhirnov V V, Myers A F, Wojak G J, Choi W B, Hren J J, Wolter S D, McClure M T, Stoner B R and Glass J T 1995 Field emission characteristics of diamond coated silicon field emitters *J. Vac. Sci. Technol. B* **13(2)** 422–426.

[42] Yen W C, Medina H C, Hsu W and Chueh Y L 2014 Conformal graphene coating on high-aspect ratio Si nanorod arrays by a vapor assisted method for field emitter *RSC Adv.* **4** 27106–111.

[43] Lv S, Li Z, Liao J, Wang G, Li M and Miao W 2015 Optimizing field emission properties of the hybrid structures of graphene stretched on patterned and size-controllable SiNWs *Sci. Rep.* **5** 15035.

[44] Jiang J, Du J, Wang Q, Zhang X, Zhu W, Li R and Yang H 2016 Enhanced field emission properties from graphene-TiO_2/DLC nanocomposite films prepared by ultraviolet-light assisted electrochemical deposition *J. Alloys and Compounds* **686** 588–92.

[45] Venkatraman V, Garg A and Peroulis D 2012 Direct measurements and numerical simulations of gas charging in microelectromechanical system capacitive switches *Appl. Phys. Lett.* **100** 083503.

[46] Venkattraman A 2015 Theory and analysis of operating modes in microplasmas assisted by field emitted cathodes *Phys. Plasmas* **22** 057102.

[47] Ilie A, Ferrari A C, Yagi T, Rodil S E, Robertson J, Barborini E and Milani P 2001 Role of sp^2 phase in field emission from nanostructured carbon *J. Appl. Phys.* **90**, 2024–2032.

[48] Carey J D, Forrest R D and Silva S R P 2001 Origin of electric field enhancement in field emission from amorphous carbon thin films *Appl. Phys. Lett.* **78(16)** 2339–2341.

[49] Ilie A, Ferrari A C, Yagi T and Robertson J, 2000 Effect of sp^2-phase nanostructure on field emission from amorphous carbons *Appl. Phys. Lett.* **76**, 2627–2629.

Table 1. Comparative table for the field electron emission characteristics of the field emitting nanostructures coated with graphene related materials.

Materials	Turn-on field (V/μm)	FEE current density (mA/cm^2)	Field enhancement factor
Graphene-silicon tip array [13]	6	3.04	1000
Graphene sheets on ZnO nanowires [14]	1.3	---	1.5×10^4
Graphene-carbon nanotube hybrids [15]	0.98	> 70	3980
Graphene-silicon nanowires [42]	2.01	---	6513
Graphene-silicon nanorod arrays [43]	8	---	423.6
Graphene-TiO_2/DLC [44]	5.2	2.95	1208
FLG-DNRs [This study]	4.21	2.24	3480

Figure captions

Figure 1. Schematics for the fabrication process of FLG-DNRs hybrids: (a) growth of NCD film on a Si substrate, (b) masking of the NCD film with ND particles, (c) reactive ion etching for forming DNRs, (d) copper coating on DNRs and (e) formation of FLG on DNRs by thermal annealing and etching of copper.

Figure 2. (a) Tilted-view SEM image of bare DNRs (inset shows the SEM morphology of the NCD film), (b) tilted-view SEM image for the FLG-DNRs hybrid with top view SEM morphology shown as inset, (c) and (d) confocal micro-Raman spectra for I. DNRs and II. FLG-DNRs, (e) HRTEM micrograph for FLG-DNRs of the designated region "I" in bright field TEM micrograph, which is shown in inset of (e) along with the corresponding selective area electron diffraction pattern, (f) HRTEM micrograph for FLG-DNRs of the designated region "II" in bright field TEM micrograph (shown in the inset of (e)). The insets FT_A–FT_B in "e" show the Fourier-transformed diffractograms corresponding to the regions marked "A" and "B" in the HRTEM image in (e), respectively, to illustrate the presence of diamond and graphene phases.

Figure 3. (a) Field electron emission current density (J_e) as a function of applied field (E) of I. DNRs and II. FLG-DNRs emitters and (b) the corresponding Fowler-Nordheim plots, i.e., *ln* (J_e/E^2)-1/E plots).

Figure 4. (a) Plasma current density (J_{PI}) and (b) photographs of plasma illumination (PI) characteristics versus applied voltage (V), and (c) plasma lifetime measurements, the plasma emission current density versus time, of a microplasma device, which utilized ITO coated glass as anode and using either I. DNRs or II. FLG-DNRs as cathode materials. The inset in (a) shows

the schematics of a microplasma device measurement setup using the FLG-DNRs hybrid as cathode. The upper inset in (c) shows the PI stability of FLG-DNRs at durations of 0 s and 1210 s, whereas the bottom inset shows the PI stability of DNRs at durations at 0 s and 938 s at an applied voltage of 650 V.

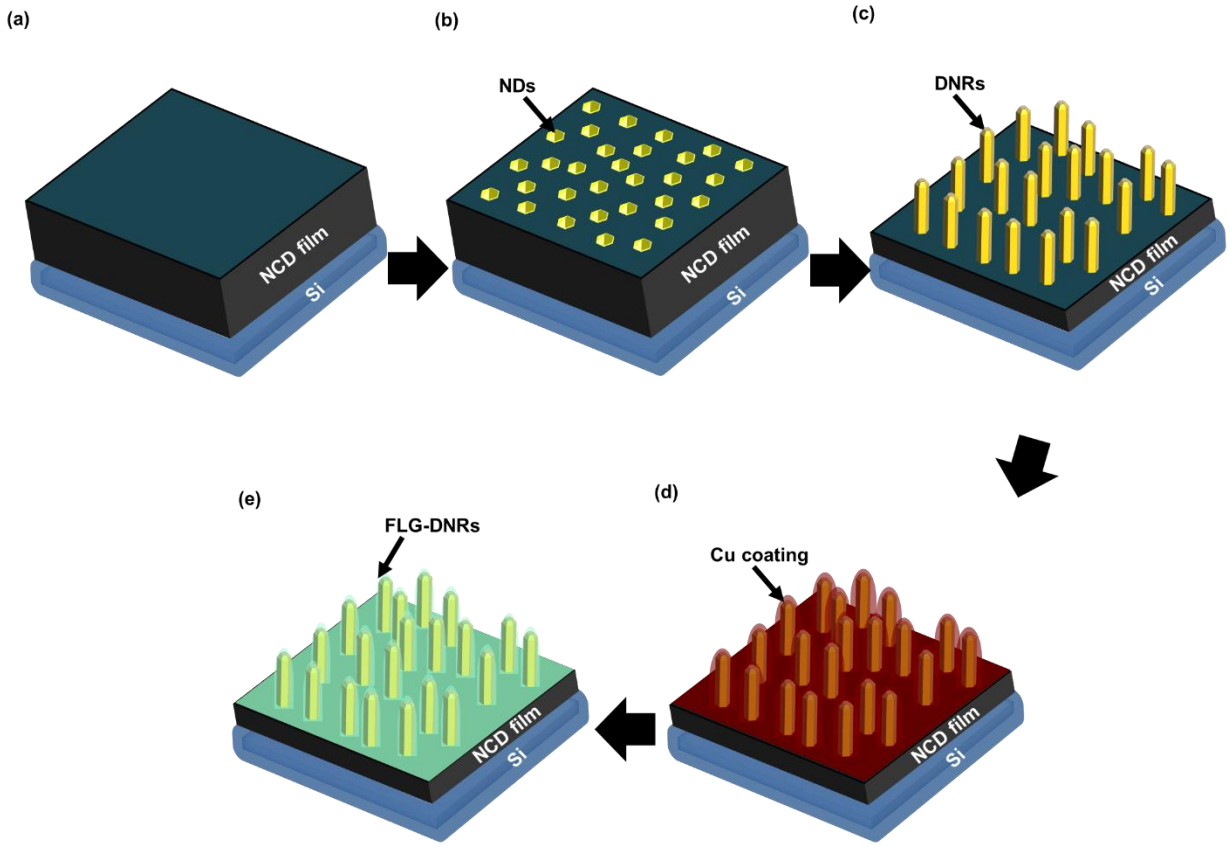

Figure 1.

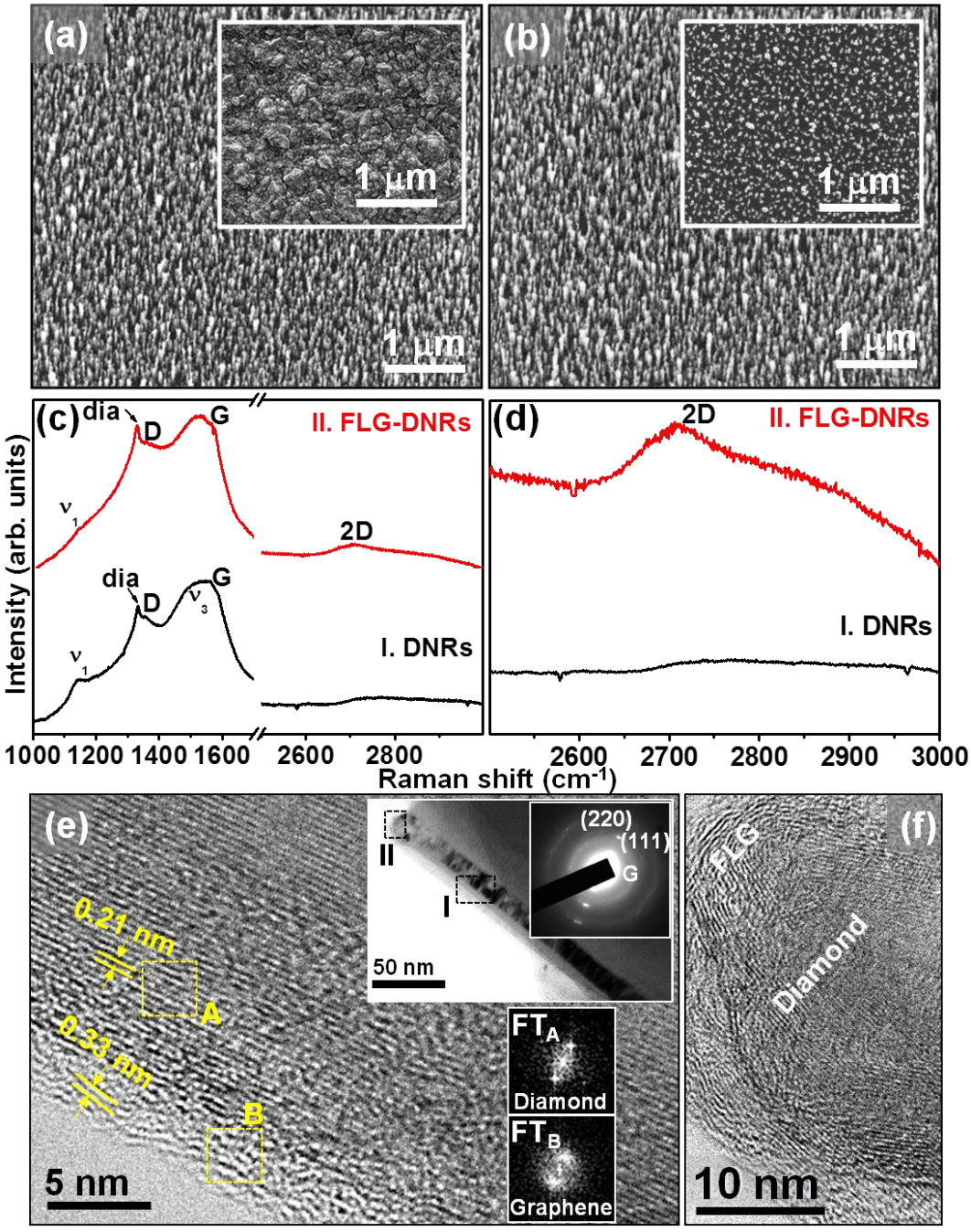
(a)
1 μm
1 μm
(b)
1 μm
1 μm
(c)
dia
D
G
II. FLG-DNRs
2D
dia
D
G
I. DNRs
Intensity (arb. units)
1000 1200 1400 1600 2600 2800
(d)
2D
II. FLG-DNRs
I. DNRs
2600 2700 2800 2900 3000
Raman shift (cm-1)
(e)
0.21 nm
A
0.33 nm
B
5 nm
II
I
50 nm
(220)
(111)
G
FTA
Diamond
FTB
Graphene
(f)
FLG
Diamond
10 nm

Figure 2.

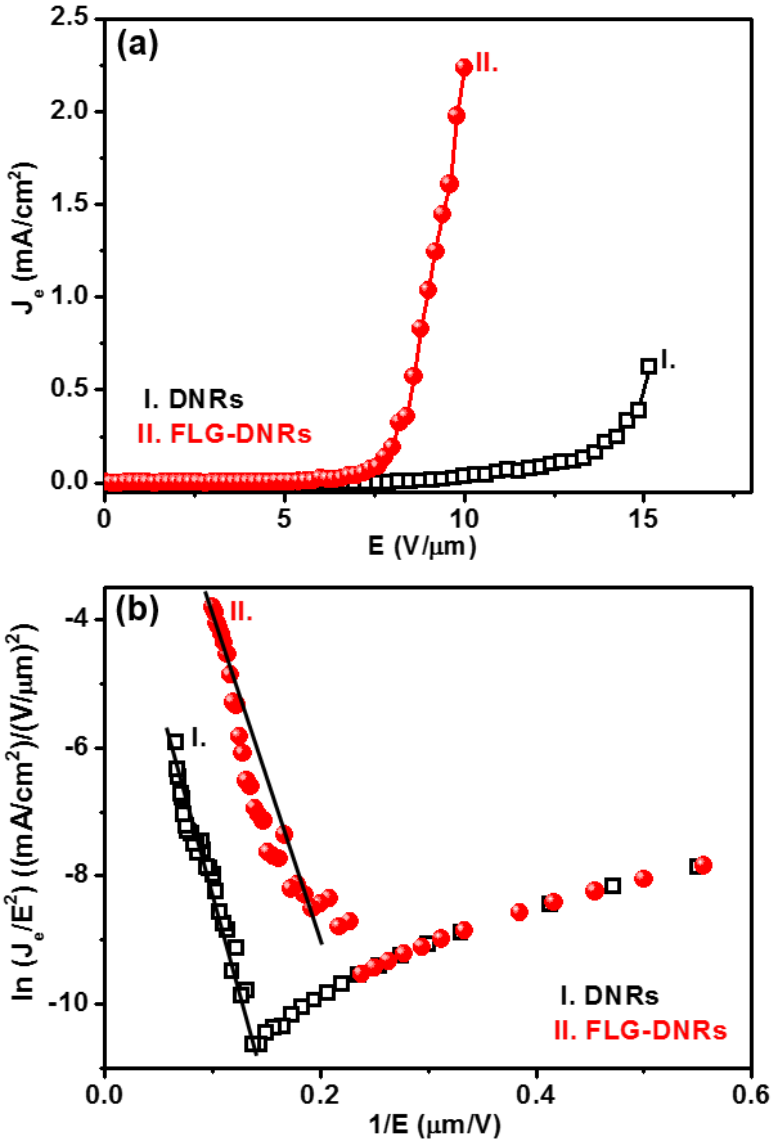
(a)
II.
I.
I. DNRs
II. FLG-DNRs
J_e (mA/cm^2)
E (V/μm)
(b)
II.
I.
I. DNRs
II. FLG-DNRs
ln (J_e/E^2) ((mA/cm^2)/(V/μm)^2)
1/E (μm/V)

Figure 3.

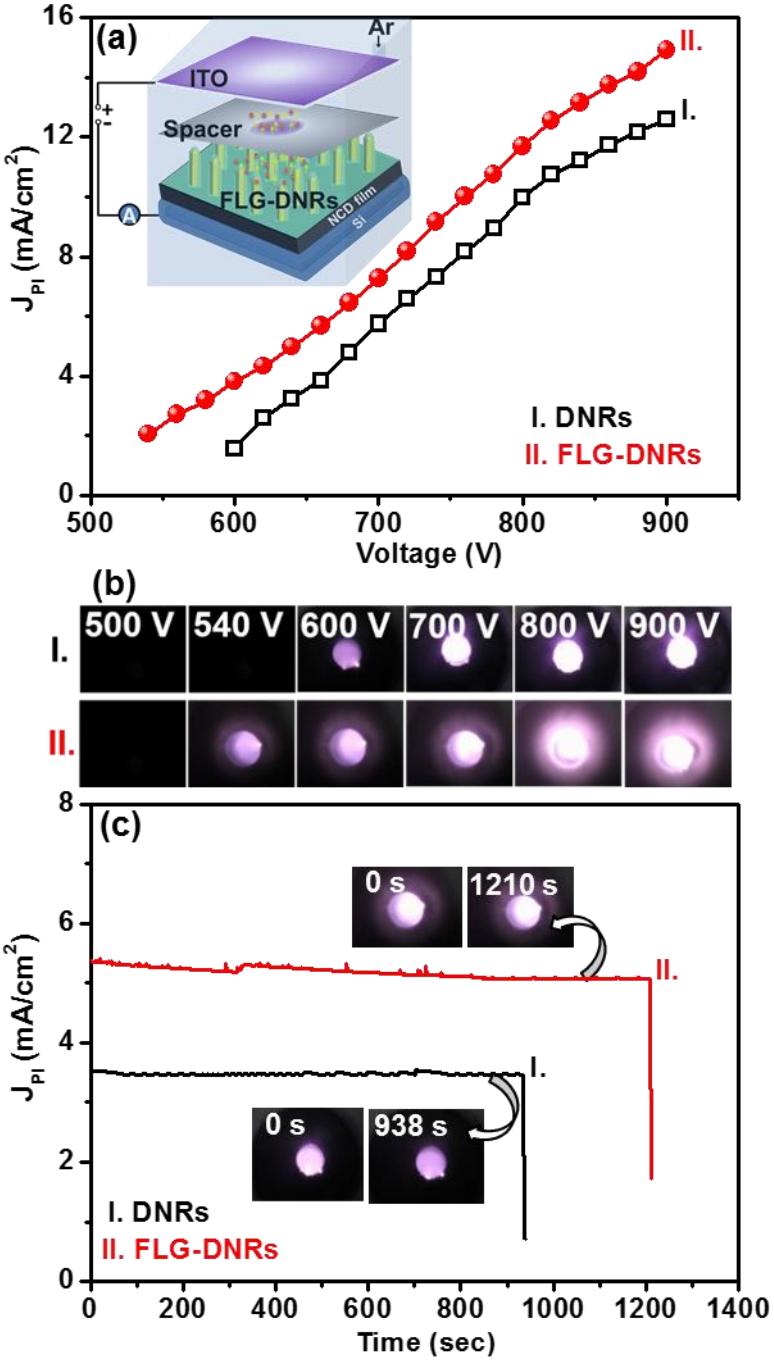
(a)
Ar
ITO
Spacer
FLG-DNRs
NCD film
Si
A
II.
I.
I. DNRs
II. FLG-DNRs
J_{PI} (mA/cm^2)
Voltage (V)
(b)
I.
II.
500 V
540 V
600 V
700 V
800 V
900 V
(c)
0 s
1210 s
0 s
938 s
I. DNRs
II. FLG-DNRs
J_{PI} (mA/cm^2)
Time (sec)

Figure 4.